Applied Mathematical Modelling 40 (2016) 3438–3446

Contents lists available at ScienceDirect

Applied Mathematical Modelling

journal homepage: www.elsevier.com/locate/apm

Cell density and cell size dynamics during *in vitro* tissue growth experiments: Implications for mathematical models of collective cell behaviour

Benjamin J. Binder[a,1], Matthew J. Simpson[b,c,*]

[a] School of Mathematical Sciences, University of Adelaide, Australia
[b] Mathematical Sciences, Queensland University of Technology (QUT), Australia
[c] Tissue Repair and Regeneration Program, Institute of Health and Biomedical Innovation (IHBI), QUT, Australia

ARTICLE INFO

Article history:
Received 18 February 2014
Revised 16 December 2014
Accepted 5 January 2015
Available online 19 February 2015

Keywords:
Cell motility
Cell proliferation
Tissue growth
Cell size
Cell density

ABSTRACT

We present a detailed experimental data set describing a tissue growth experiment where a population of cells is initially distributed uniformly, at low density, on a two-dimensional substrate, and grows to eventually form a confluent monolayer. Using image processing tools, we provide precise information about temporal changes in the number of cells, the location of cells and the total area occupied by cells. This information shows that the increase in area occupied by the cell population is affected by both the increase in cell number as well as an increase in the average size of the cells. We show that standard approaches to interpret such experiments, where the cell size is typically treated as a constant, can lead to errors. Furthermore we show that a standard, discrete, random walk model of biological cell motility and cell proliferation should not be used to represent our experimental data set since this standard model treats all cells as having a constant size that does not change with time. Instead, we introduce a generalization of the standard model which allows agents in the random walk model to move, proliferate and grow in size, and we show that the data produced by this more general model is consistent with our experimental data set.

1. Introduction

Two-dimensional tissue growth experiments are commonly used to estimate the proliferation rate of different cell types [1–9]. In these experiments a population of cells is uniformly distributed, at low density, on a two-dimensional substrate. Individual cells within the population move and proliferate, and these two processes, combined, lead to changes in the cell density and the eventual formation of a confluent monolayer of cells. Measurements obtained from these experiments can inform our understanding of wound healing [10–12] and tumor growth [13,3].

Currently, there is no standard, widely accepted methodology for the design, interpretation and quantification of tissue growth experiments. While some experiments are reported in the form of visual snapshots and qualitative comparisons [14,15], others provide more detailed cell density estimates [2,5]. A even more detailed approach is to report the precise numbers and location of individual cells [3]. Unfortunately, such a detailed approach is very labour intensive.

* Corresponding author at: Mathematical Sciences, Queensland University of Technology (QUT), Australia. Tel.: +61 7 31385241; fax: +61 7 3138 2310.
E-mail address: matthew.simpson@qut.edu.au (M.J. Simpson).
[1] Tel.: +61 7 31385241; fax: +61 7 3138 2310.

http://dx.doi.org/10.1016/j.apm.2015.01.016
S0307-904X(15)00018-9/

Typical mathematical modelling approaches used to interpret tissue growth experiments involve using a continuous logistic-type models [2,16–18,5], which can be calibrated to provide an estimate of the proliferation rate. An important limitation of using continuous models is that they neglect any explicit description of individual cell behaviour [19–25]. This limitation can be partially overcome by using discrete, random walk models. Lattice-based random walk models of two-dimensional tissue growth experiments involve placing agents on a lattice and allowing those agents to undergo motility and proliferation events, which lead to the formation a confluent monolayer [1,26,27,8,9].

In this work we present a suite of tissue growth experiments, explicitly quantifying the temporal evolution of:

(1) the number of cells per image,
(2) the location of cells within each image, and
(3) the proportion of the area of each image that is occupied by cells.

This data set allows us to investigate how the tissue growth process is influenced by the increase in cell number and changes in the cell size. The data implies that standard mathematical models could be inappropriate since standard continuous models neglect to account for any features of individual cells and standard discrete models typically assume that the average size of the cells remains constant with time. We demonstrate that care should be taken when interpreting such data since the neglect of temporal changes in cell size can lead to misinterpretations of the data. We also show that it is inappropriate to apply a standard, discrete, random walk based simulation of such a tissue growth experiment where the size of the agents in the simulation remain constant. Instead, we conclude by demonstrating how cell size dynamics could be included in a random walk model so that we can interpret this data in a more realistic modelling framework.

2. Methods

2.1. Experimental and image processing methods

All experiments in this work deal with a breast cancer cell line called MDA-MB-231 [28]. For convenience, we will refer to this cell line as 231 cells. The 231 cells were kept in Dulbecco's modified Eagle medium (Invitrogen, Australia) with 10% feotal calf serum (Hyclone, Australia) and 1% v/v Penicillin/Streptomycin (Invitrogen, Australia). The 231 cells were cultured in tissue culture flasks (Nunc, Thermo Scientific, Denmark) kept in 5% CO_2 at a temperature of 37 °C. The cells were lifted prior to confluence using 0.05% trypsin (Invitrogen, Australia) and viable cells were counted using a Trypan blue exclusion test and a haemocytometer.

A cell suspension, containing 5000 cells/100 μL, was created and carefully inserted into the wells of a 24-well tissue culture plate. Each circular well in the tissue culture place has a diameter of 15.6 mm. Initially, each well in the tissue culture plate contained 5000 cells. Cells were monitored in real time using a Leica widefield microscope. A series of images, each covering an area of approximately 640×480 μm, were recorded every 200 min over a period of 2000 min (approximately 33 h). This means that the images reported in this manuscript do not show the entire circular well in the tissue culture plate. Instead, each image shows a subregion within the circular well which means that the boundaries of the images are not physical boundaries, and the spatial extent of the cell population extends beyond the boundary of the images.

We report the physical dimensions of our experiments using a combination of microns and pixels with a conversion factor of 1.2237 μm per pixel. It is convenient to use a mixture of units since the experimental images are reported in terms of a physical scale of microns whereas the image processing is completed using a physical scale of pixels.

We denote the real dimensional time at which the images were taken as $t^* = 0,200,400,\ldots,2000$ minutes. For convenience we report the time interval using a non-dimensional timescale, $t = t^*/200$, so that our images correspond to $t = 0,1,2,\ldots,10$. Each set of experimental images corresponds to the same field of view within the tissue culture plate for the entire duration of the experiment.

We analyzed the images by determining the location of individual cells within the growing population as well as the total area of the image that is occupied by cells using customised software based on MATLAB's image processing toolbox [29,3].

3. Results

3.1. Experimental results

Images in Fig. 1 illustrate the key results from one sample of our experimental data set. Snapshots in the top row of Fig. 1 show the MDA MD 231 cells at non-dimensional time $t = 0$, 5 and 10. Initially we see that the cells are distributed approximately uniformly, at low density, and that the number of cells increases with time as a result of combined cell motility and cell proliferation processes. Results in the second row of Fig. 1 shows the approximate location of the centre of each individual cell from the experimental images in the top row. This data set clearly demonstrates the influence of cell proliferation since we have $n = 36$ cells at $t = 0$, increasing to $n = 103$ cells at $t = 100$. The images in the third row of Fig. 1 indicate, shaded in black, the area of the domain that is occupied by cells. A visual comparison of the shaded regions

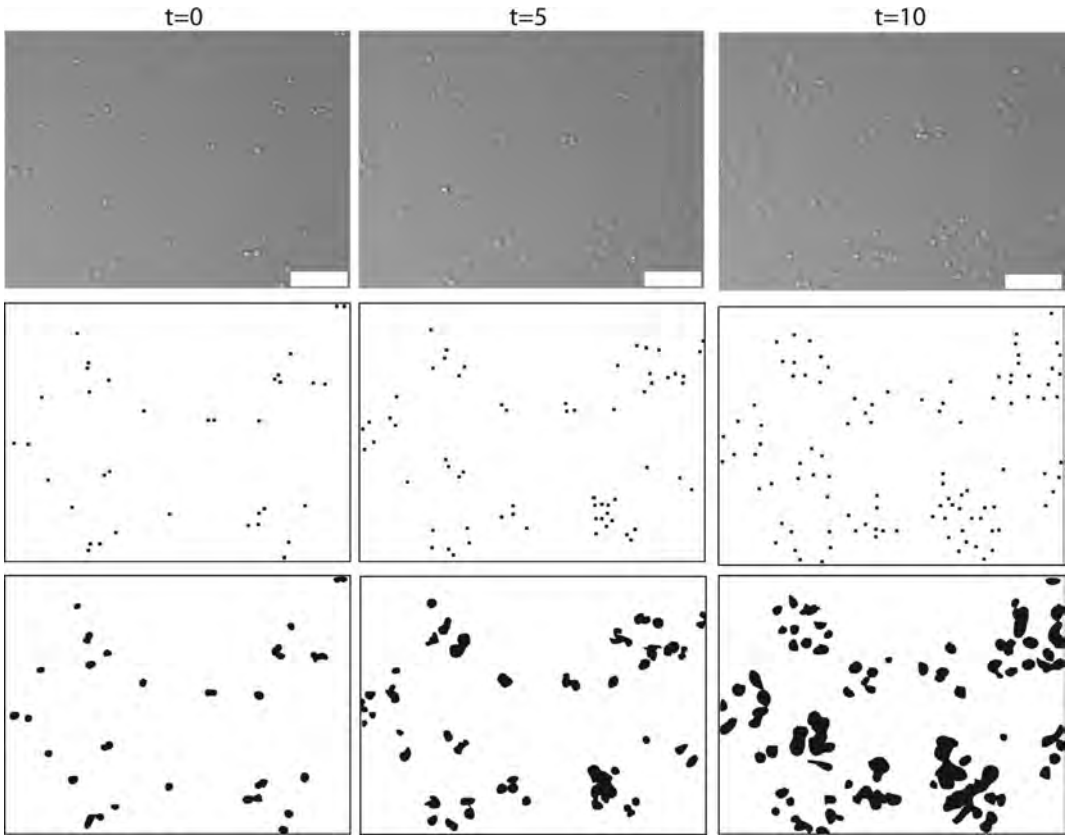

Fig. 1. Results in the top row show the raw experimental images of MDA MD 231 cells at $t = 0, 5$ and 10, respectively. The scale bar corresponds to 100 μm. The corresponding images in the second row show the location of the centre of each cell in the experimental images. This data indicates how the number of cells increases with time. Here we have $n(0) = 36$, $n(5) = 64$ and $n(10) = 103$. The images in the third row shows those regions (shaded in black) that are occupied by cells, whereas the vacant regions of the domain are not shaded.

in the third row and the original images in the top row confirms that our image analysis method provides an accurate representation of the proportion of the domain occupied by cells as a function of time.

The same image analysis, demonstrated in Fig. 1, was applied to another four identically-prepared sets of images from our experiments. This information allowed us to calculated the average number of cells per image as a function of time, $\overline{n}(t)$ and the average area of the domain that is occupied by those cells as a function of time, $\overline{A}(t)$. Using this information we can calculate the average area per cell, or the average cell size,

$$\overline{S}(t) = \frac{\overline{A}(t)}{\overline{n}(t)}. \tag{1}$$

A summary of this data set is given in Table 1, and presented graphically in Fig. 2(a) and (b).

Data in Table 1 and Fig. 2(a) indicate that $\overline{A}(t)$ is influenced by both the increase in cell number and cell size. The increase in average cell size is an interesting feature that is typically neglected by standard continuous [2,5,18] and discrete [30,1,31,3] mathematical models.

3.2. Opportunities for misinterpretation of experimental results

Given that our data set implies that the increase in the total area occupied by cells during the tissue growth experiment is influenced by both the increase in cell number and cell size, we now explore how a standard approach to interpret the results in Fig. 2(a) and (b) could lead to misinterpretations of the relevant mechanisms acting in the experiments. The data points in Fig. 2(a) shows the average cell number per image together with an exponential growth curve,

$$n(t) = n(0)\mathrm{e}^{\lambda t}, \tag{2}$$

Table 1
Average number of cells, $\overline{n}(t)$, averaged occupied area, $\overline{A}(t)$, and the averaged cell size, $\overline{S}(t)$. The averaged data is constructed from $N = 5$ identically-prepared experiments. The raw data sets, including the sample mean and sample standard deviation for each quantity are given in the Appendix.

t	$\overline{n}(t)$	$\overline{A}(t)$ (pixels)	$\overline{S}(t)$ (pixels)
0	34.60	3636.6	105.58
1	39.40	5096.6	126.65
2	46.60	6090.8	129.12
3	52.00	9082.4	173.97
4	59.40	10586	175.12
5	70.40	13323	185.34
6	84.60	14942	175.98
7	97.20	19600	200.56
8	112.20	22592	199.61
9	126.80	26335	202.39
10	131.20	30051	232.15

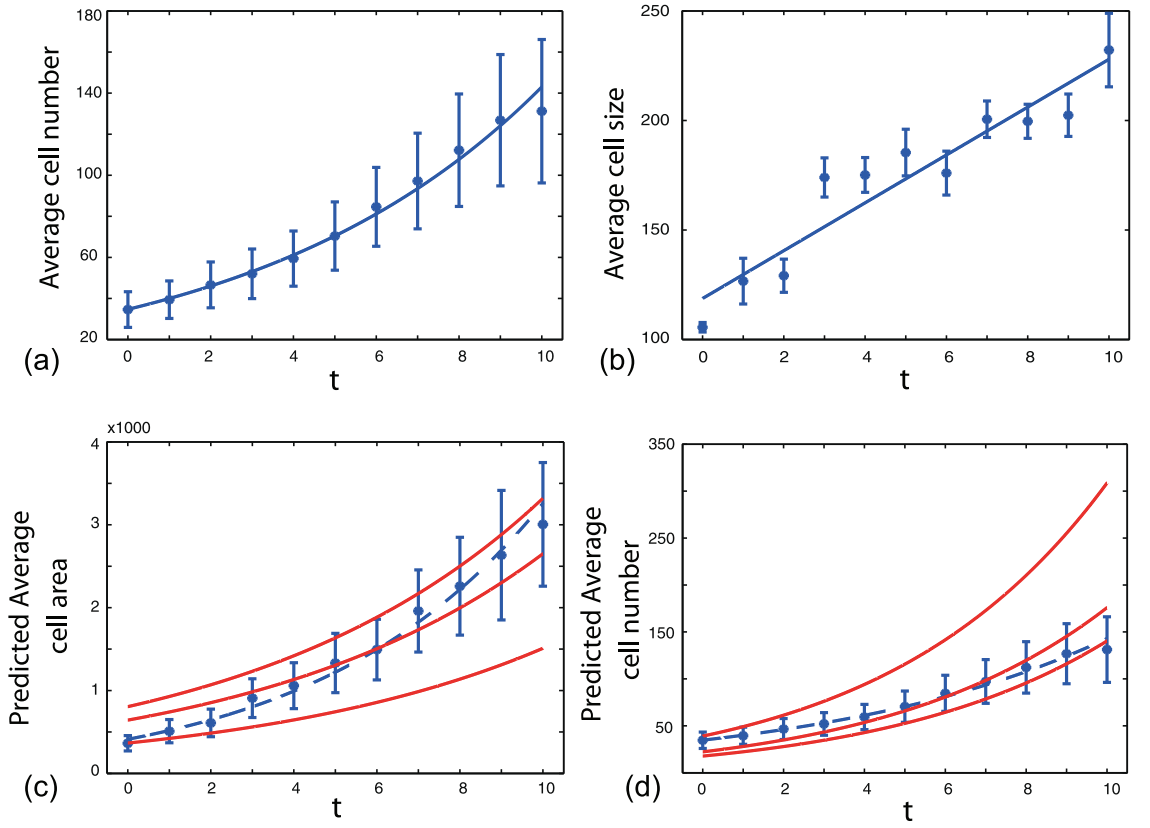

Fig. 2. (a) Data points correspond to the average numbers of cells, $\overline{n}(t)$. The solid curve is a least-squares exponential growth model, $n(t) = n(0)e^{\lambda t}$, with $n(0) = 34.7$ and $\lambda = 0.1416$. (b) Data points correspond to the average cell size, $\overline{S}(t)$. The solid curve is a least-squares linear growth curve, $S(t) = \alpha + \beta t$, with $\alpha = 118.71$ and $\beta = 10.92$. (c) Data points correspond to the total average area occupied by the cells. The three solid curves correspond to three different predictions of the total average area occupied by the cells using a standard approach neglecting any temporal changes in the average cell size, $\overline{A}(t) = \mathcal{S}\overline{n}(t)$. The lower, middle and upper predictions correspond to $\mathcal{S} = 105.58$, 185.34 and 232.15 pixels, respectively. (d) Data points correspond to the average numbers of cells. The three solid curves correspond to three different predictions of the average numbers of cells using a standard approach neglecting any temporal changes in the average cell size, $\overline{n}(t) = \overline{A}(t)/\mathcal{S}$. The lower, middle and upper predictions correspond to $\mathcal{S} = 105.58$, 185.34 and 232.15 pixels, respectively. The error-bars are for the standard error of the sample mean.

where $n(0) = 34.70$, and we estimated $\lambda = 0.1416$ to give the best match to the data. We anticipate that had the experimental data been collected for longer periods of time then we would see the numbers of cells reach an approximately steady value as crowding effects slow the net growth rate [2,5]. This kind of crowding could be represented by using a logistic, or generalised logistic growth model [17,18]; however, since we are dealing with the early time portion of the experiment before we observe any significant crowding effects, we choose to approximate this data with an exponential model.

The data points in Fig. 2(b) shows the average cell size superimposed on a linear model

$$S(t) = \alpha + \beta t, \tag{3}$$

where $\alpha = 118.71$, and we estimated $\beta = 10.92$ to give the best match to the data. The data set in Fig. 2(a) and (b), represented by the regression curves given by Eqs. (2), (3), can be used together with Eq. (1) to demonstrate now the neglect of dynamic changes in the average cell size could lead to misinterpretations of the data.

To demonstrate the potential danger in the neglect of these details we present data points in Fig. 2(c) corresponding to the measurements of the total average area occupied by cells, $\overline{A}(t)$. The three solid curves in Fig. 2(c) correspond to a simple prediction of how the average area occupied by the population of cells would change with time if we made the standard assumption that the average cell size remained constant for the duration of the experiment,

$$\overline{A}(t) = \mathcal{S}\overline{n}(t), \tag{4}$$

where $\mathcal{S}$ is the cell size, which in this case is treated as a constant. The lower solid curve in Fig. 2(c) corresponds to setting $\mathcal{S} = \overline{S}(0) = 105.58$ pixels, the middle solid curve in Fig. 2(c) corresponds to setting $\mathcal{S} = \overline{S}(5) = 185.34$ pixels, and the upper solid curve in Fig. 2(c) corresponds to $\mathcal{S} = \overline{S}(10) = 232.15$ pixels. Each solid curve in Fig. 2(c) involves implementing the standard assumption that the average cell size remains constant, and we see that in each case this leads to a significant deviation between our prediction and the observed measurements.

A second way of demonstrating the consequences of neglecting temporal changes in average cell size is to assume that we have obtained accurate estimates of the area occupied by the total population of cells, $\overline{A}(t)$ and that we have some estimate of the average cell size, $\mathcal{S}$. Using this information, together with the standard assumption that the average cell size remains constant with time, we could predict the number of cells

$$\overline{n}(t) = \frac{\overline{A}(t)}{\mathcal{S}}. \tag{5}$$

Data points in Fig. 2(d) show our measurements of $\overline{n}(t)$. The solid curves in Fig. 2(d) show the predictions made using Eq. (5). The lower curve in Fig. 2(d) corresponds to $\mathcal{S} = \overline{S}(0) = 105.58$ pixels, the middle curve corresponds to $\mathcal{S} = \overline{S}(5) = 185.34$ pixels, and the upper curve corresponds to $\mathcal{S} = \overline{S}(10) = 232.15$ pixels. Again, comparing our observed data in Fig. 2(d) with the predictions made by assuming that the average cell size remains constant indicates that this assumption could have a significant impact on our ability to correctly interpret the relevant mechanisms.

3.3. A generalised mathematical model incorporating cell motility, cell proliferation and cell growth processes

To provide a more realistic modelling framework that enables us to simulate tissue growth experiments where both the number of cells and the size of cells can increase with time, we introduce a discrete model of biological cell motility, proliferation and growth processes. The discrete model consists of a two-dimensional square lattice, with lattice spacing Δ. Lattice sites are indexed (i,j) [1,3,4] such that each lattice site is associated with a position $(x,y) = (i\Delta, j\Delta)$. The discrete model is an exclusion process [30] which explicitly incorporates crowding effects by allowing each lattice compartment to be occupied by, at most, a single agent or a portion of a single agent. For simplicity we will assume that the system of interest contains two types of agents; however, we note that this assumption can be relaxed and it is possible to generalise our model so that we can simulate any number of different types of agents. The key difference between the two types of agents that we consider is their size. For demonstrative purposes we assume that the length of type 1 agents is equal to the lattice spacing, Δ, and furthermore we assume that the agents are square so that the area of type 1 agents is Δ^2. The length of type 2 agents is equal to twice the lattice spacing, 2Δ, and each type 2 agent occupies a region corresponding to a two-by-two square arrangement of lattice sites so that the area of each type 2 agent is $4\Delta^2$. This means that a type 2 agent could occupy four adjacent sites such as (x,y), $(x+\Delta,y)$, $(x,y+\Delta)$ and $(x+\Delta,y+\Delta)$. We denote the number of type 1 agents present in the system at time t by $Q_1(t)$, and the number of type 2 agents present in the system at time t by $Q_2(t)$. The total number of agents present at time t is $Q(t) = Q_1(t) + Q_2(t)$.

Each agent in the system is motile with a transition rate P_m per unit time [1,3,4]. We suppose that motility events are unbiased so that a type 1 agent at location (x,y) will attempt to step a distance Δ to any of the four nearest neighbour lattice sites, $(x\pm\Delta,y)$, $(x,y\pm\Delta)$, with the direction of movement chosen with equal probability, 1/4. Similarly, motility events for type 2 agents are also unbiased so that a type 2 agent occupying (x,y), $(x+\Delta,y)$, $(x,y+\Delta)$ and $(x+\Delta,y+\Delta)$ attempts to step a distance Δ, with the direction of movement chosen with equal probability, 1/4. Since the model is an exclusion process any potential motility event that would place an agent, or part of an agent, on a lattice site that is already occupied by another agent will be aborted [1,3,4]. Reflecting boundary conditions are applied along all boundaries.

To model the increase in agent number, we incorporate a proliferation mechanism with rate P_p per unit time [1,3,4]. To keep our model as simple as possible we assume that only type 1 agents undergo proliferation events, but we note that this assumption could be relaxed so that both types of agents could be allowed to proliferate if necessary. Proliferation events in our model are unbiased so that a type 1 proliferative agent at location (x,y) would attempt to deposit a type 1 daughter agent at either $(x\pm\Delta,y)$ or $(x,y\pm\Delta)$ with each target site chosen with equal probability, 1/4. Any potential proliferation

event that would place a daughter agent on a lattice site that is already occupied is aborted. Similarly, any potential proliferation event that would place a daughter agent off the lattice is aborted.

Motivated by our experimental data set described in Section 3.1, we also incorporate a growth mechanism in our model so that we enable type 1 agents, each of area Δ^2, to grow into type 2 agents, each of area $4\Delta^2$. We allow this growth process to occur at rate P_g per unit time. The details of this mechanism are as follows, a type 1 agent, located at (x,y) can grow into a type 2 agent that will assume one of four potential configurations:

(1) (x,y), $(x+\Delta,y)$, $(x,y+\Delta)$ and $(x+\Delta,y+\Delta)$,
(2) (x,y), $(x-\Delta,y)$, $(x,y+\Delta)$ and $(x-\Delta,y+\Delta)$,
(3) (x,y), $(x+\Delta,y)$,$(x,y-\Delta)$ and $(x+\Delta,y-\Delta)$, or
(4) (x,y), $(x-\Delta,y)$, $(x,y-\Delta)$ and $(x-\Delta,y-\Delta)$.

For simplicity we consider an unbiased growth process where each of the four potential growth configurations is chosen with equal probability, 1/4. To ensure that our growth mechanism incorporates similar crowding principles to our motility and proliferation mechanisms, we only allow potential growth events to proceed provided that the three target sites associated with that growth event are vacant.

To illustrate the key features of this discrete model we present snapshots from two different types of simulations, on a 100×100 lattice, in Fig. 3 (a), (b), (e) and (f). The snapshot in Fig. 3(a) corresponds to a spatially uniform distribution of type 1 agents, where each lattice site is independently occupied with probability 5%. The snapshot in Fig. 3(b) corresponds to a simulation with $P_m = 1$, $P_p = 0.001$ and $P_g = 0$, so that type 1 agents are permitted to move, proliferation but not to grow. Results in Fig. 3(c) show that, on average, the number of type 1 agents increases from approximately 500 to 750, while there are no type 2 agents in the system. Using this averaged data we can calculate the average area per agent

$$\overline{A}_{\text{sim}}(t) = \frac{\overline{Q}_1(t)\Delta^2 + \overline{Q}_2(t)4\Delta^2}{\overline{Q}_1(t) + \overline{Q}_2(t)}, \tag{6}$$

where the subscript sim indicates that this average agent area corresponds to the simulation data rather than experimental data. Fig. 3(d) shows that the average area of the agents in the simulations with $P_g = 0$ remains Δ^2 for all time.

Snapshots in Fig. 3(e) and (f) are the same as in Fig. 3(a) and (b) except that we have allowed cell growth to occur. The influence of the growth process is clear by $t = 500$ since we see the appearance of larger type 2 agents in the system. Averaged simulation results in Fig. 3(g) show that the number of both type 1 and type 2 agents increases with time, and data in Fig. 3(h) quantifies how the average area per agent increases with time. Using our model we conducted simulations with

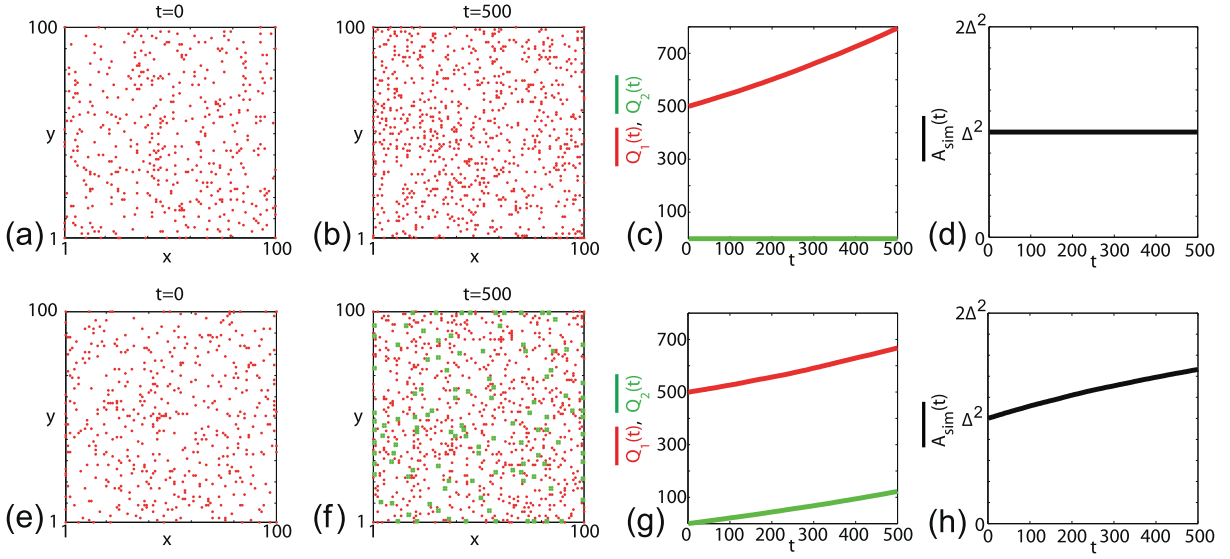

Fig. 3. Discrete modelling results. Snapshots in (a)–(b) show the results of a single simulation with $P_m = 1$, $P_p = 0.001$ and $P_g = 0.0$. The snapshots are given at $t = 0$ and $t = 500$, respectively. The smaller type 1 agents are shown in red while the larger type 2 agents are shown in green. The initial condition in (a) corresponds to a spatially uniform distribution of type 1 agents where each lattice site is initially occupied with probability 5%. Data in (c)–(d) corresponds to averaged simulation results, where the average was constructed using 100 identically-prepared realizations of the same stochastic process. Snapshots in (e)–(f) show the results of a single simulation with $P_m = 1$, $P_p = 0.001$ and $P_g = 0.0005$. The snapshots are given at $t = 0$ and $t = 500$, respectively. The initial condition in (e) corresponds to a spatially uniform distribution of type 1 agents where each lattice site is initially occupied with probability 5%. Data in (g)–(h) corresponds to averaged simulation results, where the average was constructed using 100 identically-prepared realizations of the same stochastic process. (For interpretation of the references to color in this figure legend, the reader is referred to the web version of this article.)

Table 2
Cell number data from $N = 5$ samples. The cell number in each image is n_i, for $i = 1, 2, 3, 4, 5$. The sample average number of cells, $\overline{n}(t)$, and the sample standard deviation, $\sigma_n(t)$, are given.

t	n_1	n_2	n_3	n_4	n_5	$\overline{n}(t)$	$\sigma_n(t)$
0	36	17	34	66	20	34.60	19.44
1	41	22	38	72	24	39.40	20.04
2	55	25	46	84	23	46.60	24.97
3	55	30	52	95	28	52.00	27.01
4	57	34	60	109	37	59.40	30.05
5	64	39	76	131	42	70.40	37.21
6	87	46	84	154	52	84.60	42.94
7	94	55	95	184	58	97.20	52.12
8	100	61	110	216	74	112.20	61.26
9	109	67	130	247	81	126.80	71.50
10	103	71	135	264	83	131.20	78.09

Table 3
The area occupied by cells from $N = 5$ samples. The total area occupied by cells in each sample, A_i, is reported for $i = 1, 2, 3, 4, 5$. Area measurements are reported in pixels and the domain size is $X \times Y = 523 \times 391 = 204493$ pixels, with 1.2237 μm/pixel. The sample mean, $\overline{A}(t)$, and the sample standard deviation, $\sigma_A(t)$, are given.

t	A_1	A_2	A_3	A_4	A_5	$\overline{A}(t)$	$\sigma_A(t)$
0	3511	1878	3591	7055	2148	3636.6	2062.3
1	3856	2408	5430	10357	3432	5096.6	3135.3
2	5667	3043	6432	12185	3127	6090.8	3725.2
3	8063	4984	8872	17963	5530	9082.4	5228.9
4	8404	6236	10873	21146	6273	10586	6202.5
5	9837	6463	15531	26293	8493	13323	7994.3
6	12118	7955	16668	28338	9631	14942	8176.7
7	16183	10579	20766	38157	12315	19600	11090
8	17031	12024	23355	45017	15534	22592	13190
9	18723	14413	26480	56432	15626	26335	17469
10	24413	13269	30814	57676	24081	30051	16679

Table 4
Data for the average cell size from $N = 5$ samples. The average size of the cells in each sample is $S(t)_i = A(t)_i/n(t)_i$ for $i = 1, 2, 3, 4, 5$. The sample mean, $\overline{S}(t)$, and sample standard deviation, $\sigma_S(t)$, are given.

t	S_1	S_2	S_3	S_4	S_5	$\overline{S}(t)$	$\sigma_S(t)$
0	97.53	110.47	105.62	106.89	107.40	105.58	4.84
1	94.05	109.45	142.89	143.85	143.00	126.65	23.37
2	103.04	121.72	139.83	145.06	135.96	129.12	16.96
3	146.60	166.13	170.62	189.08	197.50	173.97	20.02
4	147.44	183.41	181.22	194.00	169.54	175.12	17.75
5	153.70	165.72	204.36	200.71	202.21	185.34	23.81
6	139.29	172.93	198.43	184.01	185.21	175.98	22.41
7	172.16	192.35	218.59	207.38	212.33	200.56	18.60
8	170.31	197.11	212.32	208.41	209.92	199.61	17.39
9	171.77	215.12	203.69	228.47	192.91	202.39	21.63
10	237.02	186.89	228.25.25	218.47	290.13	232.15	37.54

different P_m, P_p and P_g which showed that the average change in cell size is sensitive to the choice of parameters and we expect that this information could be used, together with the data presented previously in Fig. 2(b), to calibrate this kind of model.

While our discrete model has been designed to mimic certain key features of our experimental dataset, such as the increase in average cell size with time, we would like to make it clear that several generalizations of our model are possible. For example, here we only consider a population composed of two types of agents whereas it might be more reasonable to deal with a discrete model with many more types of agents. Similarly, we consider the simplest possible proliferation mechanism where the smallest agents in the model produce daughter agents of the same size and we neglected to allow the larger agents to proliferate. Many other potential proliferation mechanisms could be considered, including more general agent growth mechanisms whereby agents of area Δ^2 increase in size to agents of area $2\Delta^2$. One of the limitations of this kind of growth process is that agents of area $2\Delta^2$ are not symmetric with respect to the underlying lattice and so if this option were followed we would have to account for the alignment of these asymmetric subpopulations. One way of overcoming this issue is to focus only on subpopulations that are symmetric with respect to the lattice. Another way of overcoming

this issue would be to use a lattice-free modelling framework [32–35]. Here we chose to use a lattice-based framework since lattice-free simulation tools are far more computationally demanding.

4. Discussion and conclusions

In this work we presented an experimental data set describing a two-dimensional tissue growth experiment which leads to the formation of a confluent monolayer of cells. To analyze the experimental data set we used image processing tools to provide precise information about how number, location and total area occupied by cells changes with time. Our data set shows that the increase in area occupied by the growing population of cells is affected by both the increase in cell and size. Most models used to interpret two-dimensional tissue growth experiments do not apply to our experimental data. Standard continuous models neglect to account for individual-level properties, and standard discrete models assume that the size of the agents does not change dynamically [30,36,37,27,38,39,34,31,8,9].

We proposed a simple discrete model of motility, proliferation and growth to mimic our data set. When the cell growth rate is set to zero, our discrete model makes similar predictions to other models [1,3,4] and these predictions can not be used to match our experimental data. Alternatively, when we incorporate growth, our discrete simulations predict that both the numbers and size of agents increases with time. This information, that is lacking in previous models, could be used to match our experimental data set.

Finally, our discrete modelling results in this work have been presented in terms of single snapshots of the stochastic process and averaged data obtained by considering many identically-prepared realizations of the same stochastic process. An area of great interest to the mathematical biology community is to understand how the averaged properties of a particular discrete process can be described using continous models such as ordinary differential equations and partial differential equations [30,20,1,40–42]. While some previous work has been completed on understanding how to derive approximate differential equation description of systems with different sized agents [43,44], none of these previous studies considered systems that were composed of several types of different sized agents like we have shown in Fig. 3(e) and (f). We suggest that a thorough exploration deriving appropriate continuous limits of these kinds of discrete processes with multi-sized agents will be a fruitful avenue for future research.

Acknowledgements

We appreciate support from the Australian Research Council (FT130100148), the National Health and Medical Research Council (APP1069757), and the School of Mathematical Sciences at QUT who provided funding for BJB to visit QUT.

Appendix A. Experimental data set

The data set in Table 2 describes the number of cells in each image, together with the sample mean and the sample standard deviation.

The data set in Table 3 describes the area occupied by cells in each image, together with the sample mean and the sample standard deviation.

The data set in Table 4 describes average area per cell in each sample, together with the sample mean and the sample standard deviation.

References

[1] R.E. Baker, M.J. Simpson, Correcting mean-field approximations for birth-death-movement processes, Phys. Rev. E 82 (2010) 041905.
[2] A.Q. Cai, K.A. Landman, B.D. Hughes, Multi-scale modeling of a wound-healing cell migration assay, J. Theor. Biol. 245 (2007) 576.
[3] M.J. Simpson, B.J. Binder, P. Haridas, B.K. Wood, K.K. Treloar, D.L.S. McElwain, R.E. Baker, Experimental and modelling investigation of monolayer development with clustering, Bull. Math. Biol. 75 (2013) 871.
[4] M.J. Simpson, J.A. Sharp, R.E. Baker, Distinguishing between mean-field, moment dynamics and stochastic descriptions of birth–death-movement processes, Phys. A 395 (2014) 236.
[5] A. Tremel, A. Cai, N. Tirtaatmadja, B.D. Hughes, G.W. Stevens, K.A. Landman, A.J. O'Connor, Cell migration and proliferation during monolayer formation and wound healing, Chem. Eng. Sci. 64 (2009) 247.
[6] D.C. Walker, J. Southgate, G. Hill, M. Halcombe, D.R. Hose, S.M. Wood, S. MacNeil, R.H. Smallwood, The epitheliome: agent-based modelling of the social behaviour of cells, Biosystems 76 (2004) 89.
[7] D.C. Walker, G. Hill, S.M. Wood, R.H. Smallwood, J. Southgate, Agent-based computational modelling of wounded epithelial cell monolayers, IEEE Trans. Nanobiosci. 3 (2004) 153.
[8] K. Zygourakis, R. Bizios, P. Markensooff, Proliferation of anchorage-dependent contact-inhibited cells: 1. Development of theoretical models based on cellular automata, Biotech. Bioeng. 38 (1991) 459.
[9] K. Zygourakis, P. Markensooff, R. Bizios, Proliferation of anchorage-dependent contact-inhibited cells: II. Experimental results and validation of the theoretical models, Biotech. Bioeng. 38 (1991) 471.
[10] P.D. Dale, P.K. Maini, J.A. Sherratt, Mathematical modelling of corneal epithelial wound healing, Math. Biosci. 124 (1994) 127.
[11] P.K. Maini, D.L.S. McElwain, D.I. Leavesley, Traveling wave model to interpret a wound-healing cell migration assay for human peritoneal mesothelial cells, Tissue Eng. 10 (2004) 475.
[12] P.K. Maini, D.L.S. McElwain, D.I. Leavesley, Travelling waves in a wound healing assay, Appl. Math. Lett. 17 (2004) 575.
[13] J.A. Sherratt, Wavefront propagation in a competition equation with a new motility term modelling contact inhibition between cell populations, Proc. R. Soc. A 456 (2000) 2365.

[14] V. Krishnan, L.A. Shuman, D.M. Sosnoski, R. Dhurjati, E.A. Volger, A.M. Mastro, Dynamic interaction between breast cancer cells and osteoblastic tissue: comparison of two-and three-dimensional cultures, J. Cell Physiol. 226 (2010) 2150.
[15] C. Merceron, S. Portron, M. Masson, J. Lesoeur, B.H. Fellah, O. Gauthier, O. Geffroy, P. Weiss, The effect of two-and three-dimensional cell culture on the chondrogenic potential of human adipose-derived mesenchymal stem cells after subcutaneous transplantation with an injectable hydrogel, Cell Transplant. 20 (2011) 1575.
[16] S.A. Maggelakis, A mathematical model of tissue replacement during epidermal wound healing, Appl. Math. Model. 27 (2003) 189.
[17] J.D. Murray, Mathematical Biology I: An Introduction, Springer, Heidelberg, 2002.
[18] A. Tsoularis, J. Wallace, Analysis of logistic growth models, Math. Biosci. 179 (2002) 21.
[19] A.R.A. Anderson, M.A.J. Chaplain, Continuous and discrete mathematical models of tumor-induced angiogenesis, Bull. Math. Biol. 60 (1998) 857.
[20] R.E. Baker, C.A. Yates, R. Erban, From microscopic to macroscopic descriptions of cell migration on growing domains, Bull. Math. Biol. 72 (2009) 719.
[21] E.A. Codling, M.J. Plank, S. Benhamou, Random walks in biology, J. R. Soc. Interface 5 (2008) 813.
[22] C. Guiot, P.G. Degiorgis, P.P. Delsanto, P. Gabriele, T.S. Deisboeck, Does tumour growth follow a universal law? J. Theor. Biol. 225 (2003) 147.
[23] H.G. Othmer, S.R. Dunbar, W. Alt, Models of dispersal in biological systems, J. Math. Biol. 26 (1988) 263.
[24] S. Turner, J.A. Sherratt, K.J. Painter, N.J. Savill, From a discrete to a continuous model of biological cell movement, Phys. Rev. E 69 (2004) 021910.
[25] G.B. West, J.H. Brown, B.J. Enquist, A general model for ontogenic growth, Nature 413 (2001) 628.
[26] G. Cheng, B.B. Youssef, P. Markenscoff, K. Zygourakis, Cell population dynamics modulate the rates of tissue growth processes, Biophys. J. 90 (2006) 713.
[27] Y. Lee, S. Kouvroukoglou, L.V. McIntire, K. Zygourakis, A cellular automaton model for the proliferation of migrating contact-inhibited cells, Biophys. J. 69 (1995) 1284.
[28] R. Cailleau, R. Young, M. Olivé, W.J. Reeves Jr., Breast tumor cell lines from pleural effusions, J. Nat. Cancer Inst. 53 (1974) 661.
[29] B.J. Binder, M.J. Simpson, Quantifying spatial structure in experimental observations and agent-based simulations using pair-correlation functions, Phys. Rev. E 88 (2013) 022705.
[30] G. Ascolani, M. Badoul, C. Deroulers, Exclusion processes: short-range correlations induced by adhesion and contact interactions, Phys. Rev. E 87 (2013) 012702.
[31] B.G. Sengers, C.P. Please, R.O.C. Oreffo, Experimental characterization and computational modelling of two-dimensional cell spreading for skeletal regeneration, J. R. Soc. Interface 4 (2007) 1107.
[32] S.T. Johnston, M.J. Simpson, M.J. Plank, Lattice-free descriptions of collective motion with crowding and adhesion, Phys. Rev. E 88 (2013) 062720.
[33] M.J. Plank, B.D. Sleeman, Lattice and non-lattice models of tumour angiogenesis, Bull. Math. Biol. 66 (2004) 1785.
[34] M.J. Plank, M.J. Simpson, Models of collective cell behaviour with crowding effects: comparing lattice-based and lattice-free approaches, J. R. Soc. Interface 9 (2012) 2983.
[35] M.J. Plank, M.J. Simpson, Lattice-free models of cell invasion: discrete simulations and travelling waves, Bull. Math. Biol. 75 (2013) 2150.
[36] B.J. Binder, K.A. Landman, M.J. Simpson, M. Mariani, D.F. Newgreen, Modeling proliferative tissue growth: a general approach and an avian case study, Phys. Rev. E 78 (2008) 031912.
[37] B.J. Binder, K.A. Landman, Exclusion processes on a growing domain, J. Theor. Biol. 259 (2009) 541.
[38] D.C. Markham, M.J. Simpson, R.E. Baker, Simplified method for including spatial correlations in mean-field approximations, Phys. Rev. E 87 (2013) 062702.
[39] K.J. Painter, T. Hillen, Volume-filling and quorum-sensing in models for chemosensitive movement, Can. Appl. Math. Quart. 10 (2002) 501.
[40] L. Dyson, P.K. Maini, R.E. Baker, Macroscopic limits of individual-based models for motile cell populations with volume exclusion, Phys. Rev. E 86 (2012) 031903.
[41] K.A. Landman, A.E. Fernando, Myopic random walkers and exclusion processes: single and multispecies, Phys. A 390 (2011) 3742.
[42] C.A. Yates, R.E. Baker, R. Erban, P.K. Maini, Going from microscopic to macroscopic on nonuniform growing domains, Phys. Rev. E 86 (2012) 021921.
[43] C.J. Penington, C. Korvasova, B.D. Hughes, K.A. Landman, Collective motion of dimers, Phys. Rev. E 86 (2012) 051909.
[44] M.J. Simpson, R.E. Baker, S.W. McCue, Models of collective cell spreading with variable cell aspect ratio: a motivation for degenerate diffusion models, Phys. Rev. E 83 (2011) 021901.